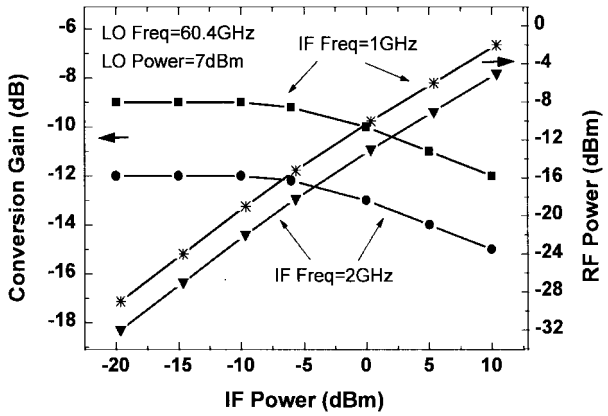

Fig. 8. Up-converter conversion gain and RF output power versus IF power.

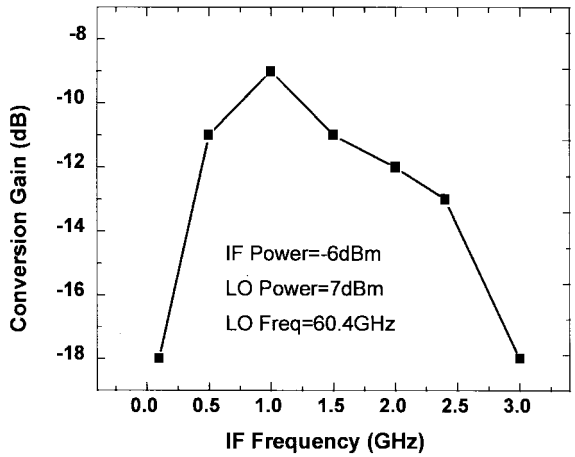

Fig. 9. Up-converter conversion gain versus IF frequency.

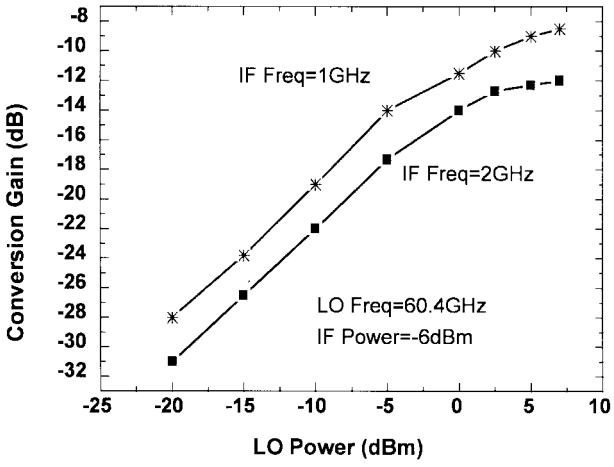

Fig. 10. Up-converter conversion gain versus LO power.

applied to the source terminal. With an LO power and frequency of 7 dBm and 60.4 GHz, both converters can operate at any IF frequency within 0.5–2 GHz, with a corresponding conversion gain within -7 to -12 dB, which is primarily dominated by the related filter's insertion loss. The frequency converters reported in this paper are expected to find applications in millimeter-wave wireless LAN systems.

REFERENCES

[1] R. A. Pucel, D. Masse, and R. Bera, "Performance of GaAs MESFET mixers at X-band," *IEEE Trans. Microwave Theory Tech.*, vol. MTT-24, pp. 351–360, June 1976.

[2] C. C. Penalosa and C. Aichison, "Analysis and design of MESFET gate mixer," *IEEE Trans. Microwave Theory Tech.*, vol. MTT-35, pp. 643–652, July 1987.

[3] P. Bura and R. Dikshit, "FET mixer with the drain LO injection," *Electron. Lett.*, vol. 12, no. 20, pp. 536–537, Sept. 1976.

[4] G. Tomassetti, "An unusual microwave mixer," in *Proc. European Microwave Conf.*, Dublin, Ireland, Sept. 1986, pp. 754–757.

[5] V. Brady, T. Hsu, R. Reeves, and M. Vermeulen, "Development of a monolithic FET Ka-band single side band up-converter and image reject down-converter," in *IEEE GaAs IC Symp. Dig.*, San Diego, CA, Oct. 1989, pp. 189–192.

[6] W. R. Brinlee, A. M. Pavio, C. L. Goldsmith, and W. J. Thompson, "A monolithic multifunction EW broad-band receiver converter," in *IEEE GaAs IC Symp. Dig.*, San Jose, CA, Oct. 1993, pp. 207–210.

[7] T. Hirota and M. Muraguchi, "K-band frequency up-converters using reduced-size couplers and dividers," in *IEEE GaAs IC Symp. Dig.*, Monterey, CA, Oct. 1991, pp. 53–56.

[8] A. Minakawa and T. Hirota, "An extremely small 26-GHz monolithic image-rejection mixer without DC power consumption," *IEEE Trans. Microwave Theory Tech.*, vol. 41, p. 1634–1637, Sept. 1993.

[9] M. Madihian, L. Desclos, K. Muruhashi, K. Onda, and M. Kuzuhara, "A monolithic AlGaAs/InGaAs up-converter IC for K-band wireless networks," *IEEE Trans. Microwave Theory Tech.*, vol. 43, pp. 2773–2778, Dec. 1995.

Physical Scaling Rules for AlGaAs/GaAs Power HBT's Based on a Small-Signal Equivalent Circuit

U. Schaper and P. Zwicknagl

***Abstract*—Physical scaling rules for AlGaAs/GaAs heterojunction bipolar transistors (HBT's) containing 2–16 emitter fingers are demonstrated. The parameter extraction is based on a small-signal equivalent circuit. The scaling parameters compare favorably with the measured data from the process control monitor.**

***Index Terms*—Heterojunction bipolar transistor, parameter extraction, scaling rules, small-signal model.**

I. INTRODUCTION

GaAs-based heterojunction bipolar transistors (HBT's) are promising power devices for L-band (mobile telephone) and X-band (radar) applications. Based on a T-shaped small-signal equivalent circuit, scaling rules for multifinger power HBT's have been derived to allow for the optimization of multiemitter cell design and monolithic microwave integrated circuits (MMIC's). Each circuit element is assigned a physical property by comparison with the equivalent circuit of the HBT topology. The derived physical scaling rules hold not only for various emitter areas [1], but also for all critical device design parameters. As a result, the rules can be used to evaluate multifinger unit cells [2] and provide feedback for process control data.

Manuscript received February 27, 1997; revised April 7, 1998.

The authors are with Siemens AG, Corporate Technology, Department ZT KM 5, D-81730 Munich, Germany (e-mail: ulrich.schaper@mchp.siemens.de).

Publisher Item Identifier S 0018-9480(98)04947-3.

TABLE I
SCALING RESULTS AND COMPARISON WITH PROCESS DATA. FOR THE DETERMINATION OF CONTACT RESISTIVITIES, THE TRANSFER LENGTH L_T IS USED. COLLECTOR AND SUBCOLLECTOR LAYERS OF THE DEVICE ARE REPRESENTED IN THE EQUIVALENT CIRCUIT BY ONE ELEMENT, THE COLLECTOR SHEET RESISTANCE R_C. THE MEASURED JUNCTION CAPACITIES DEPEND ON THE JUNCTION VOLTAGES. THE SCALING RULES SHOW THAT THE APPLIED VOLTAGE IS ACTIVE ONLY FOR THE INTRINSIC DEVICE

Small Signal Model Parameter	Scaling Rule	Process Data
Specific contact resistivities		
emitter	$\rho_0 = 1.5 \cdot 10^{-6}\ \Omega cm^2$	$1.2 \cdot 10^{-6}$ ... $1.3 \cdot 10^{-6}\ \Omega cm^2$
base	$\rho_1 = 8.1 \cdot 10^{-6}\ \Omega cm^2$	$6.4 \cdot 10^{-6}$ ... $13 \cdot 10^{-6}\ \Omega cm^2$
collector	$\rho_2 = 2.7 \cdot 10^{-5}\ \Omega cm^2$	$1.3 \cdot 10^{-6}\ \Omega cm^2$ ($L_T = 1.3\ \mu m$)
		$2.8 \cdot 10^{-5}\ \Omega cm^2$ ($L_T = 6\ \mu m$)
Interconnection inductances		
emitter	$L_0 = 0.25\ pH + 20\ pH / n_E$	
base	$L_1 = 38\ pH + 35\ pH / n_E$	$0.55 pH/\mu m \rightarrow 42\ pH$
collector	$L_2 = 29\ pH + 45\ pH / n_E$	$0.70 pH/\mu m \rightarrow 36\ pH$
Sheet resistances:		
base	$R_{B\square} = 330\ \Omega/\square$	250 ... 320 $\Omega/\square$
collector	$R_{C\square} = 250\ \Omega/\square$	coll.: 710 $\Omega/\square$
		sub-coll.: 10 $\Omega/\square$
Specific junction capacities:		
external base-collector	$C_F/A = 0.42\ fF/\mu m^2$	0.42 ... 0.48 $fF/\mu m^2$ (0 V)
internal base-collector	$C_Q/A = 0.18\ fF/\mu m^2$	0.20 $fF/\mu m^2$ (3 V)
Output and emitter resistance		
	$R_Q = 2.9\ k\Omega + 21\ k\Omega / n_E$	
	$R_E = 0.088\ \Omega + 0.78\ \Omega / n_E$	
Current source		
	$\alpha_0 = 0.965 - 0.070 \cdot 10^{-3} \cdot A_E / \mu m^2$	$1 - 1/\beta = 0.967$
	$F_{3dB} = 31\ GHz - 0.012\ GHz \cdot A_E / \mu m^2$	

II. POWER DEVICE

The power HBT's are fabricated by the Siemens HBT process on 3-in AlGaAs/GaAs wafers grown by metal–organic chemical-vapor disposition (MOCVD). The key steps of this process are: 1) photolithography performed by i-line stepper; 2) device mesa isolation by dry etching; 3) perfectly flat planarization using plasma-enhanced silicon nitride; 4) ohmic contact: Ni/Ge/Au for the n-contact and Pt/Ti/Pt/Au for the p-contact; and 5) wafer thinning down to 100 μm. A cross section of the HBT along with the layer thicknesses and doping levels is shown in Fig. 1. A fishbone-type layout (see Fig. 2) has been chosen, which is characterized by two rows of transistor cells. The transistor bases are fed through a central metallization. The collectors are connected and combined to the right of the figure and the emitter contacts are supplied from the top and bottom sides. All transistor terminals are connected by airbridges. Typical data for the HBT with 120-μm^2 emitter area at current density $j_C = 5 \cdot 10^4$ A/cm^2 and $V_{CE} = 3$ V are: 1) current gain $\beta = 20$–30; 2) transit frequency $f_T > 30$ GHz; and 3) base–collector breakdown voltage $V_{\mathrm{BCO}} = 20$ V.

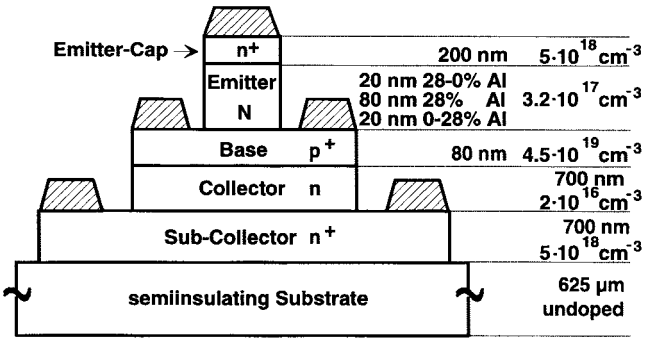

Fig. 1. Schematic cross section of the AlGaAs/GaAs HBT with layer thicknesses and doping levels.

III. METHOD

The physical scaling rules are based on an equivalent circuit (see Fig. 3), the elements of which can be related to the cross section of the device (see Fig. 1). The element pairs (L_1, R_1), (L_2, R_2), and (L_0, R_0) describe the interconnect inductance and the contact resistance of the device terminals base, collector, and emitter, respectively. The sheet resistance of base and collector are given by R_B and R_C based on the current path from the internal device to the ohmic contacts. The base–collector junction capacitances are C_F and C_Q for the external and internal parts of the junction. The output resistance R_Q is in parallel to the current source driven by the emitter current I_E. The current source is described by the dc emitter-to-collector current ratio $\alpha_0 = I_E/I_C$ and the 3-dB corner-frequency $F_{3\mathrm{dB}}$. The remaining parameter R_E and C_E characterize the base–emitter junction. The resistance R_E is a function of the emitter current through the forward-biased diode, the capacitance C_E describes the transit time.

Parameter extraction based on the previously reported analytical method [3] has been applied to S-parameters measured from 1 to 26 GHz. HBT's with emitter lengths from 20 to 30 μm, emitter widths from 2 to 3 μm, and emitter finger numbers n_E from 2 to 16 were used. Thus, the total emitter area varies by a factor of eight from 120 to 960 μm^2. The diced HBT's belong to several wafers and have been depicted at random from different areas of the wafer. For the derivation of scaling rules, the HBT's are operated under bias conditions suitable for a comparison. Each HBT was biased at $V_{CE} = 3$ V with a collector current density of $j_C = 5 \cdot 10^4$ A/cm^2,

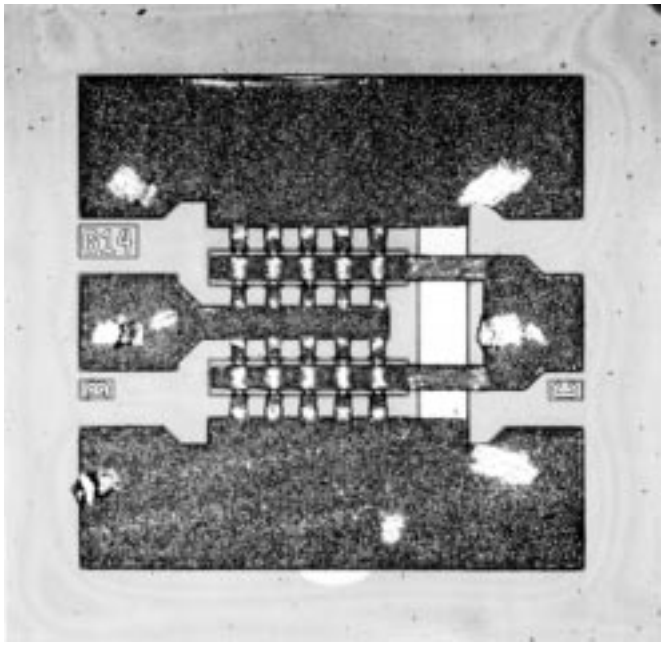

Fig. 2. Fishbone-type multifinger HBT with 2 × 5 HBT cells.

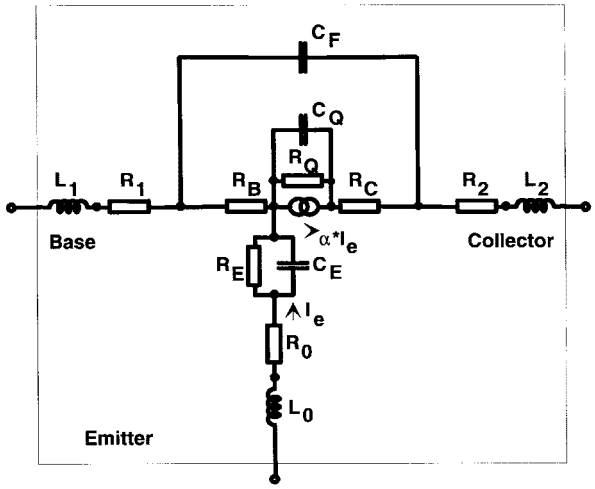

Fig. 3. Small-signal equivalent circuit.

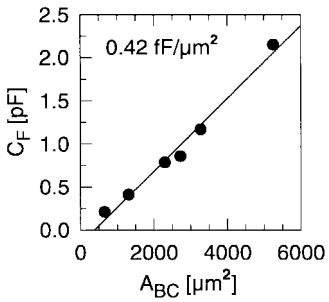

Fig. 4. External base–collector junction capacitance C_F versus base–collector junction area A_{BC}.

which is a typical bias point for power applications. The current density instead of the current is held constant for each HBT to achieve almost equal operating conditions, including the self-heating effect. The scaling rules are not restricted to this chosen bias point, they apply equally well in the active range of the HBT.

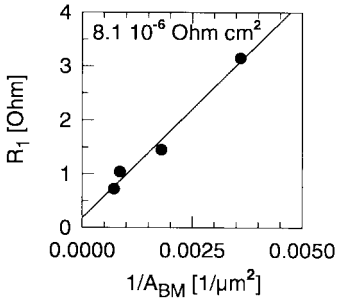

Fig. 5. Base contact resistance R_1 versus the inverse of the base contact area A_{BM}.

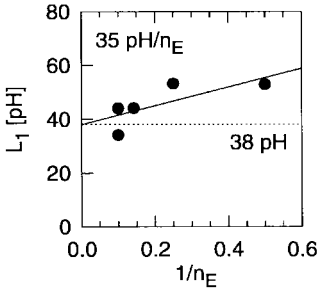

Fig. 6. Base series inductance L_1 versus the inverse of the number n_E of emitter fingers. Each transistor base contact is fed from a central line of metallization, which is seen here as an inductance offset of 38 pH.

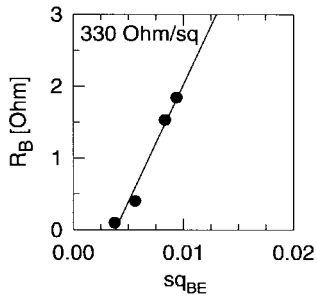

Fig. 7. Base sheet resistance R_B versus number of squares sq_{BE} between base and emitter.

IV. Results

The key point of the analysis is to plot the small-signal model parameters versus their appropriate geometrical parameter: junction area, contact area, contact length, and contact distance or number of fingers. This analysis represents the physical nature of the device and reveals the close link of the equivalent circuit of the active device and the process data measured on test structures of the process control monitor. The result of this analysis are physical scaling rules. Several examples are given in the following figures (the complete data are listed in Table I). The external base–collector capacitance C_F is plotted versus the base–collector junction area A_{BC} (see Fig. 4) giving a specific capacitance of 0.42 fF/μm^2. The base contact resistance R_1 is proportional to the inverse of the base contact area A_{BM} (see Fig. 5) resulting in a specific contact resistivity ρ_1 of $8.1 \cdot 10^{-6}\ \Omega \cdot \text{cm}^2$. The base series inductance L_1 is split into the part for the central feed line, which is seen as an offset in L_1 and the part which is dependent on the number of fingers used in the transistor (see Fig. 6). The sheet resistance R_B depends on the base–emitter spacing shown as a function of the number of squares sq_{BE} between base and emitter contacts (see Fig. 7). This dependence is determined

to be 330 $\Omega/\square$. Thus, for each model parameter, a scaling rule is derived. These scaling rules are compared with the process data in Table I. The process parameters are determined from test structures of the process control monitor of the Siemens HBT process. The process data range, e.g., for the base contact, includes variations both of process inhomogeneity and base layer properties along a whole wafer. The deviations of the small-signal model parameters from the regression line are due to the arbitrary selected sample. Nevertheless, the scaling parameters compare favorably with the process data, the agreement being better than 10%. The bias condition served as a basis for the derivation of the scaling rules; these rules are not restricted to this bias point, they apply to the normal active region of the transistor. The self-heating effect of the HBT is considered in two aspects. First, the HBT's are operated under constant current density to achieve almost equal conditions for a comparison. Second, the larger the HBT area, the more pronounced the self-heating effect for the device. This feature is captured in the decrease of the current source parameters α_0 and $F_{3\mathrm{dB}}$ with the increase of the area (see Table I).

V. Conclusion

Physical scaling rules for AlGaAs/GaAs power HBT's with 2–16 emitter fingers of 120–960-$\mu\mathrm{m}^2$ emitter areas have been developed. The parameter extraction method was based on a small-signal T-shaped equivalent circuit. From the small-signal model, scaling rules with scaling parameters has been established based on the physical interpretation of each equivalent circuit parameter. The scaling parameters compare favorably with the measured data from the process control monitor. The scaling rules can provide a basis for layout of power transistors and for the control of critical performance parameters.

References

[1] D.-W. Wu, M. Fukuda, Y.-H. Yun, and D. L. Miller, "Small-signal equivalent circuit scaling properties of AlGaAs/GaAs HBT's," in *IEEE MTT-S Int. Microwave Symp. Dig.*, Orlando, FL, May 14–19, 1995, pp. 631–634.

[2] R. Hajji, F. M. Ghannouchi, and A. B. Kouki, "A systematic layout-based method for the modeling of high-power HBT's using the scaling approach," *IEEE Trans. Electron Devices*, vol. 42, pp. 528–533, Mar. 1995.

[3] U. Schaper and B. Holzapfl, "Analytical parameter extraction of the HBT equivalent circuit with T-like topology from measured S-parameters," *IEEE Trans. Microwave Theory Tech.*, vol. 43, pp. 493–498, Mar. 1995.

Calibration and Verification of the Pure-Mode Vector Network Analyzer

David E. Bockelman and William R. Eisenstadt

***Abstract*—In this paper, the calibration of a pure-mode vector network analyzer (PMVNA) is presented in detail. The analyzer is intended for the measurement of mixed-mode scattering parameters (s-parameters) of differential circuits, but is also suitable for measurement of general microwave networks with up to four ports. The theory of calibration of the analyzer is developed in terms of a general n-port analyzer, including the correction of port-to-port crosstalk. The type of the standards used in calibration is examined, and the minimum number of standards are summarized for various levels of crosstalk correction. A new standard—called a generalized through, desirable for all multiport network analyzer calibrations—is introduced. A calibration is performed from 0.25 to 25.25 GHz based on standards with coaxial connectors, and verification standards are measured. The measured data is compared with National Institute of Standards and Technology (NIST) traceable measurements, and errors are found to generally less than ± 1 dB in transmission. In many cases, the error is less than the uncertainty of the NIST traceable measurements.**

***Index Terms*—Calibration, measurement, measurement standards, networks.**

I. Introduction

Differential circuits are becoming increasingly important in radio frequency (RF) and microwave applications, particularly in integrated circuits (IC's). The differential circuit topology is being widely adopted in RF IC's due to its crosstalk immunity and increased dynamic range over ground-referenced circuits. This increase in differential applications at RF has lead to the development of scattering parameter (s-parameter) based characterization of these circuits, known as mixed-mode s-parameters [1].

Accurate measurements are ultimately required for any RF differential application, but the measurement of differential circuits has been a significant problem. Recently, a new specialized vector network analyzer (VNA) system has been developed for the measurement of differential circuits [2]. This new analyzer, called a pure-mode VNA (PMVNA), stimulates and measures the device under test (DUT) with the two fundamental modes of differential circuit operation: the differential mode and the common mode. Special considerations required for the accurate calibration of the PMVNA and the results of a practical implementation of the PMVNA calibration are presented in this paper. This paper is organized as follows. In Section II, the error model of the PMVNA is presented and the basic calibration equation is given. The removal of switching effects is also covered in this section. Section III provides details of the solution of the calibration problem. Section IV presents measured results and verification through comparison to National Institute of Standards and Technology (NIST) traceable data, and conclusions are given in Section V.

Manuscript received February 28, 1997; revised April 7, 1998.

D. E. Bockelman is with Motorola Radio Products Applied Research, Plantation, FL 33322 USA (e-mail: d.bockelman@ieee.org).

W. R. Eisenstadt is with the University of Florida, Gainesville, FL 32611 USA.

Publisher Item Identifier S 0018-9480(98)04946-1.